Solar Energy 288 (2025) 113294

Contents lists available at ScienceDirect

Solar Energy

journal homepage: www.elsevier.com/locate/solener

Statistical methods for assessment of energy harvesting performance in unconventional photovoltaics

Mikhail Vasiliev [a,*], Victor Rosenberg [a], James Bullock [b], Paul Mulvaney [c]

[a] ClearVue Technologies Ltd Perth Australia
[b] Department of Electrical and Electronic Engineering, University of Melbourne, Parkville, VIC 3010, Australia
[c] ARC Centre of Excellence in Exciton Science, School of Chemistry, University of Melbourne, Parkville, VIC 3010, Australia

ARTICLE INFO

Keywords:
Photovoltaics
Window-integrated
Agrivoltaics
Energy harvesting
Renewables

ABSTRACT

Results of long-term monitoring of the energy harvesting trends in field-installed large area luminescent solar concentrator based windows are reported. The main features and materials-related aspects of these unconventional, window-integrated photovoltaics are described, together with the laboratory techniques used to rate their performance. New statistical methods suitable for benchmarking the season-dependent and design-dependent field performance characteristics are described. Key performance differences between conventional and LSC based photovoltaics are identified using long-term observational datasets. Experimental results show that windows equipped with 3D structured PV modules and fluorescent polymer interlayers often feature higher energy yield stability in adverse weather conditions compared to roof-mounted silicon panels. A new parameter proposed for the quantification of the energy yield stability reveals strong advantages of the wall-mounted and mixed-orientation window-integrated PV over the conventional roof-mounted systems. The datasets also reveal correlations between the energy yield performance and window design types. The proposed data analysis methods are expected to help identify the best material combinations for use in commercial-size LSCs, complementing the standard lab assessments made using small-area samples.

1. Introduction

Buildings use a third of the world's energy [1] and, as a result, there is growing interest in the potential of building integrated photovoltaic systems (BIPV) [2 –9]. City buildings often lack roof space and have large glazing areas and consequently window-integrated photovoltaics (WIPV) has emerged as an interesting and challenging target for the BIPV research community. Within this field, the most unconventional and hence challenging idea has been the creation of ***transparent*** WIPV systems, i.e. windows which offer both high visible-range transparency and simultaneous power generation [10]. This clearly necessitates the use of novel optical materials and glazing system structures [11–16]. Such high-transparency PV windows provide an attractive combination of energy savings and on-site renewable electricity generation [16,17]. It has been reported that photovoltaic windows could reduce annual energy use and CO_2 footprints by 40 % and enable net-zero energy buildings [18]. Recent efforts have focused on maximizing the building energy savings through the application of advanced glazing practices [19] and through the optimization of photovoltaic system designs, particularly in building-integrated settings [20–22]. To date, the approach which is most common is based on luminescent solar concentrators (LSC) [23–33].

In an LSC based WIPV, a luminescent molecule, nanocrystal or phosphor is used to absorb incident solar energy and to re-radiate it as fluorescence. Energy collection occurs in slab-shaped waveguides and these are typically performance-rated by measuring the current–voltage (I-V) characteristics under solar illumination in small-scale (eg 100 mm x 100 mm) concentrator samples. However, the efficiency of a slab is strongly dependent on the slab dimensions. As a result, lab based measurements on small samples (e.g. 10 cm x 10 cm) do not adequately predict performance in full scale windows. Such large, window-integrated PV systems require a range of methods for their field performance prediction and benchmarking, not all of which have yet been standardized. For convenience, it is useful to distinguish between conventional and unconventional BIPV systems. Window-integrated PV systems can be considered unconventional if any additional energy harvesting mechanisms (eg, luminescence, scattering, or diffraction) are utilized, compared with conventional BIPV. In conventional PV and

* Corresponding author.
E-mail address: mikhail@clearvuepv.com (M. Vasiliev).

https://doi.org/10.1016/j.solener.2025.113294
Received 7 October 2024; Received in revised form 9 December 2024; Accepted 17 January 2025

BIPV systems the conversion of solar energy to electricity occurs at the point of light incidence. Conversely, in WIPV systems, internal light redirection or optical energy redistribution mechanisms are employed, which utilise the 3D space available inside the window glazing systems. Consequently, the energy harvesting mechanisms in high-transparency solar windows depend on both the absorber material and on the optical properties of the window itself and the spatial disposition of PV cells assembled along the rim to harvest the light energy. ClearVue LSC components are assembled as ultra-clear, low-iron glass laminates using polyvinyl butyral (PVB) interlayers containing inorganic rare-earth-doped luminophore particles.

However, despite extensive laboratory scale studies of LSCs, there are few detailed reports on the energy production trends for practical WIPV systems [4,5,20–22,34–36]. Such studies are complex and even roof-mounted, silicon-based modules subjected to real-world weather and lighting variations can exhibit energy efficiencies significantly different from the expected values [37]. Hence there is a need to carry out studies of the environmental response of LSC [13,38,39] or hybrid systems using LSC components [16,17,40]. The emergent field of unconventional photovoltaics can be broadly defined as a group of energy generation technologies reliant on novel combinations of solar energy materials, optical and optoelectronic systems, and physical principles employed for the photon collection, which have not yet been widely deployed or commercialized. In recent years, there has been a strong and growing research interest in all areas of unconventional photovoltaics, including the development of novel spectral converters of solar radiation, quantum dot materials for use in luminescent solar concentrators, large-area LSC performance up-scaling, and the development of standardized protocols for the evaluation of LSC performance [41–47].

This manuscript focusses on results from field testing a number of LSC based WIPV systems. In April 2021, a research greenhouse was constructed at Murdoch University (Perth, Australia), featuring three types of high-transparency PV windows. These windows were slightly different in their fluorescent interlayer material combinations and also had varying phosphor concentrations. The windows were manufactured by ClearVue Technologies Ltd. Each solar window was constructed as a triple-glazed insulated glass unit containing a 3D arrangement of near-perimeter, strip-shaped, silicon-based PV modules [15], a fluorescent particle-loaded polyvinyl butyral (PVB) interlayer which provides internal light redistribution through both luminescence and light scattering [10,25,26], and a low-emissivity (heat mirror) optical coating. Technical details related to this solar greenhouse and some initial results of the energy output and energy use monitoring have been reported in [10] and [17]. The findings made during the first two years of greenhouse PV operation have provided useful insights into the response of the solar windows to varying environmental parameters, including solar incidence geometry and weather conditions. Significant energy savings provided by the combination of solar energy generation and insulation-related thermal energy savings compared to a conventionally glazed room are demonstrated. In addition, new methods for the identification

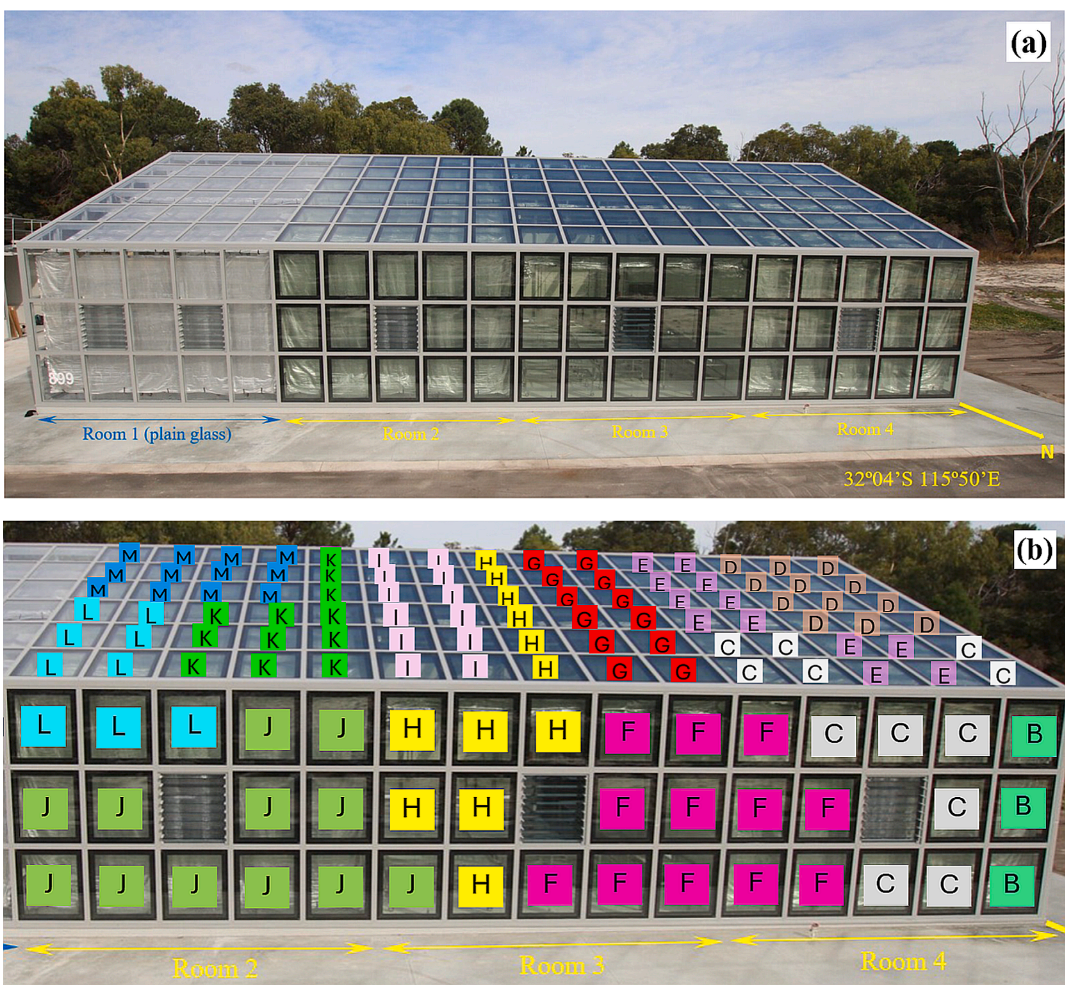

Fig. 1. (a) Murdoch University solar greenhouse featuring high-transparency triple-glazed solar photovoltaic windows. **(b)** Arrangement of multiple window-integrated PV arrays across the greenhouse building envelope. Arrays (coded alphabetically, with a 12-window Array A mounted across the western wall not shown in diagram) feature parallel-connected PV window bundles; each array was connected to one Enphase IQ7 + microinverter for AC conversion, energy monitoring, and grid linkage.

of energy harvesting differences in solar window modules are shown to be possible through longer-term data processing and observations [17].

2. Background and methods

Fig. 1 shows the greenhouse structure, which is composed of four grow-rooms with differing glazing designs. Note that rooms 2–4 were fitted with PV windows. Also shown is the arrangement of the different window groups into separate PV arrays distributed across the building envelope (northern and western sides). A total of 153 PV windows of size 1.1 m × 1.2 m were integrated into the greenhouse building envelope. All window arrays (except Array L) were composed of 12 windows each; some of the arrays needed to be distributed across differently oriented surfaces. For example, Array B had 3 windows mounted on the north wall with the rest on the west wall. Depending on the sample-to-sample manufacturing (assembly and component) quality variations and window design types, the rated power outputs (corresponding to the factory measured STC flash-test characterization results) varied from ∼ 27 to 30 W_p/m^2. In the field some windows generated up to ∼ 33 W_p/m^2 under near-noon sunlight irradiation, when oriented at optimized azimuth and tilt angles (which, notably, did not correspond to normal incidence).

Fig. 2 details several laminated fluorescent device types and the results of benchmarking based on LSC I-V curve measurements made with edge-attached silicon cells.

The amounts of solar energy harvested by the array installed at the Murdoch University Solar Greenhouse were data-logged continuously and stored online, enabled by an Enphase Envoy Communication Gateway and Enphase Enlighten online data access interface. Multiple energy production-related parameters were data-logged on each array, including the date-specific and time-dependent electric outputs (current and voltage at the maximum-power point, instantaneous active power, etc.). The instantaneous, daily, or time-cumulative energy production output dependencies were also logged. Multiple datasets were obtained and analyzed during this study, which involved an observation period of over three years. The effects of window design and window orientation on the peak-power and energy harvesting outputs were reported in [17].

3. Results and discussion

The following sections summarize the energy harvesting results obtained after processing array datasets collected between 01 May 2021 – 27 May 2024. We compare the data to the performance of a conventional roof-mounted PV system; some datasets also make a comparison with an older solar window installation on a north-facing vertical wall in Perth. Solar window design differences between the three solar rooms of greenhouse are related only to the number of fluorescent interlayers and their luminophore types and particle concentrations. Table 1 specifies the interlayer types and sequences used in each room and lists the relevant window arrays. Note that "PVB-1" and "PVB-2" interlayers each contained a mix of two inorganic rare earth activated luminophores (based on oxide and sulfide composition types). PVB-2 interlayers had a larger particle loading concentration of both luminophore materials,

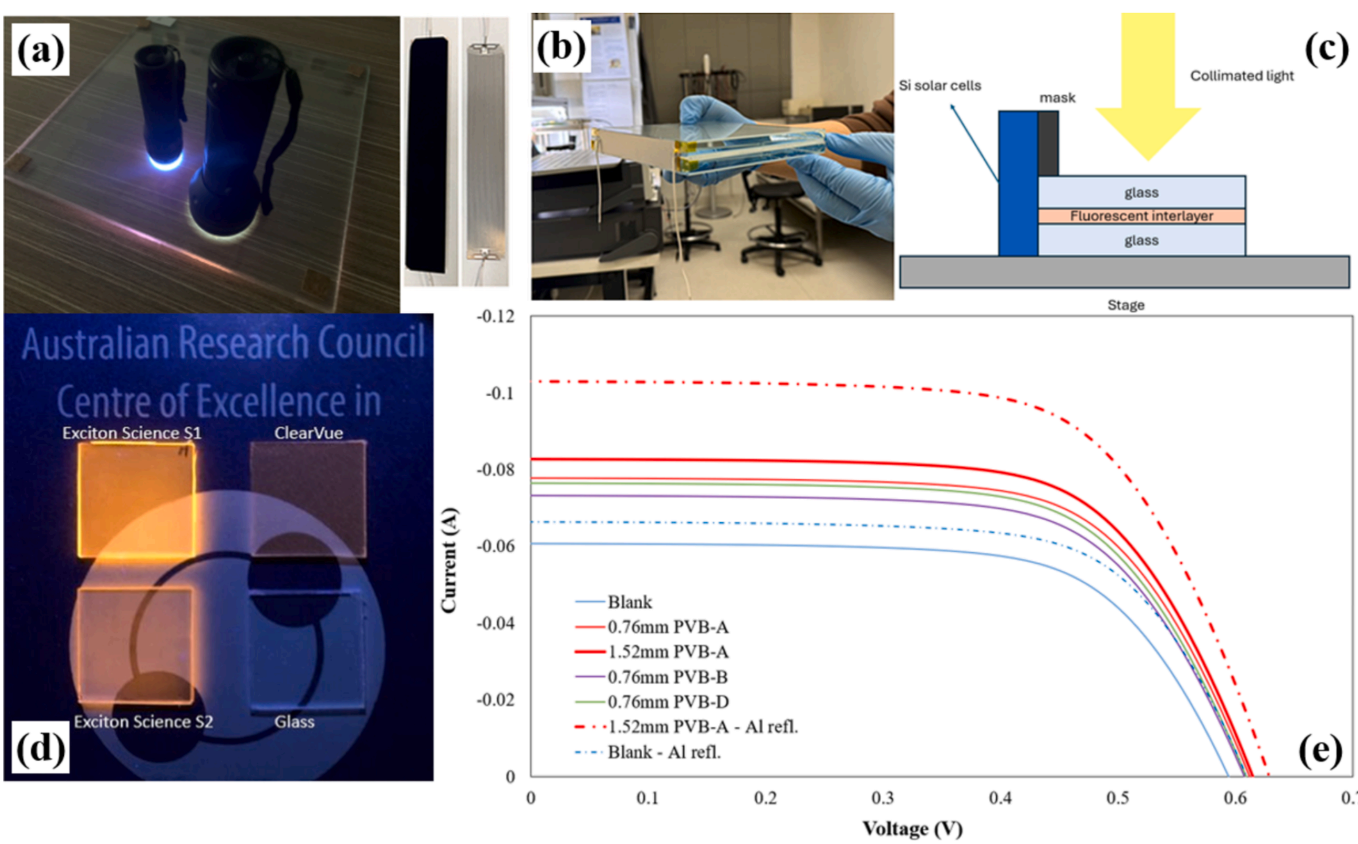

Fig. 2. Glass-based PVB-laminated luminescent concentrator components and their characterization. (a) Image of the energy conversion, light spreading, and edge concentration effects in a 30 cm x 30 cm x 0.9 cm fluorescent glass laminate under long-wave UV LED excitation. (b) Efficiency-calibrated strip-shaped silicon cell cut-outs and small-scale glass laminates with solar cell strips covering edge area used in lab characterization experiments. (c) Geometry of test LSC exposure used in I-V curve measurements with normally-incident solar simulator light. (d) Small luminophore-doped laminate samples and low-iron glass under λ = 365 nm UV exposure featuring a ClearVue microparticle-loaded interlayer and interlayers containing CdSe@ZnS quantum dots. ClearVue interlayers have a peak wavelength of fluorescence excitation away from λ = 365 nm, therefore the relative visual brightness comparisons do not directly represent the relative performance scaling. (e) PV I-V curves measured in 100 mm x 100 mm x 12 mm concentrators made using 3 different ClearVue material types and blank samples; the effects of placing a reflective aluminium layer under the bottom glass surface are also shown.

Table 1
Interlayer-related glazing system design differences between the three solar grow-rooms and window PV arrays distribution.

Solar room ID	Fluorescent interlayer type(s)	Window arrays
Room 2	Two 0.76 mm PVB-2 interlayers separated by 4 mm of glass within a 12 mm-thick middle pane of triple glazing	J, K, L, M
Room 3	1 0.76 mm PVB-1 interlayer and 1 0.76 mm PVB-2 interlayer	F, G, H, I, J
Room 4	1 0.76 mm PVB-1 interlayer and 1 0.76 mm blank interlayer	A,B, C, D, E, F

also featuring stronger light scattering effects, compared with PVB-1.

3.1. Long-term observations and data analysis

Long-term daily energy production datasets were collected from the Murdoch University solar greenhouse as well as from a conventional roof-mounted PV system rated at 6.6 kW_p. Each of the datasets was analyzed to quantify the percentage of days during which the daily energy production exceeded a set percentage of the maximum-observed daily energy production amount, in steps of 5 %. The results are presented graphically in Fig. 3.

The data region related to the top 20 % of the maximum observed daily energy outputs is quite descriptive of the systems performance during the environmental exposure conditions close to the optimum conditions for PV energy harvesting. The data from this region allow an at-a-glance separation of the data traces belonging to the roof-, wall-mounted, and mixed arrays, since during the sunny clear days with strong near-noon solar radiation intensity conducive to efficient energy collection, the optimally tilted roof areas have an advantage in energy collection efficiency compared to the vertical wall surfaces. At the same time, conventional PV on the optimally oriented roof surface clearly outperforms all windows in terms of the probability of producing the highest (top quintile) possible daily energy outputs during the most favourable weather conditions. This may be due to several factors, such as the exposure of window-integrated PV components to higher ambient air temperatures inside sealed window air spaces and their lower efficiency when there is significant wind-induced convective cooling. Additionally, the greater the incoming sunlight energy density, the more it will be dissipated inside the energy-absorbing fluorescent interlayers, considering the finite fluorescent materials quantum yields and modest efficiencies of photon collection for the light rays not incident (or refracted) directly onto any PV surfaces. These factors will always limit the practically achievable photon collection efficiency in WIPVs, particularly in the case of high-transparency, clear PV windows designed to minimize haze and visible-range transmission losses. A recent study reported in [28] focusing on the applications potential of luminescent concentrators also concluded that standard PV systems outperform even the best available LSC systems in energy production, with the latter category possessing distinct advantages of its own, related to more efficient collection of diffuse and indirectly-incident light.

Near the top 20 % energy harvesting boundary, it can be seen clearly that the roof-mounted arrays provide this top-quintile performance much more frequently (over all seasons) compared to the wall-roof mixed arrays (dashed lines), and all wall-mounted arrays. Interestingly, the data traces from the wall-mounted arrays A and F practically coincide for the region within top 25 % of energy production, despite their significantly different azimuthal orientations. This may be due to the similarities in the incidence angle-dependent peak-power producing orientations of both (slightly different in their interlayer compositions) window design types; all windows of similar triple-glazed design types featured the peak output power when inclined by 10-15° from the normal incidence, in both planes. The data traces from the north wall-mounted windows of slightly different glazing design types (arrays J, C, and F) start to diverge notably from one another already below the region of top 15–20 % of daily outputs. These differences can be explained by the design-dependent variations in the electric power output at larger angles of solar radiation incidence, which would be magnified on the north-facing wall, with the increasing sunlight intensity near noon falling obliquely onto glass surfaces. This is also confirmed by the season-dependent responses of the peak noon-time power outputs to the variations in the solar radiation incidence geometry studied in [17].

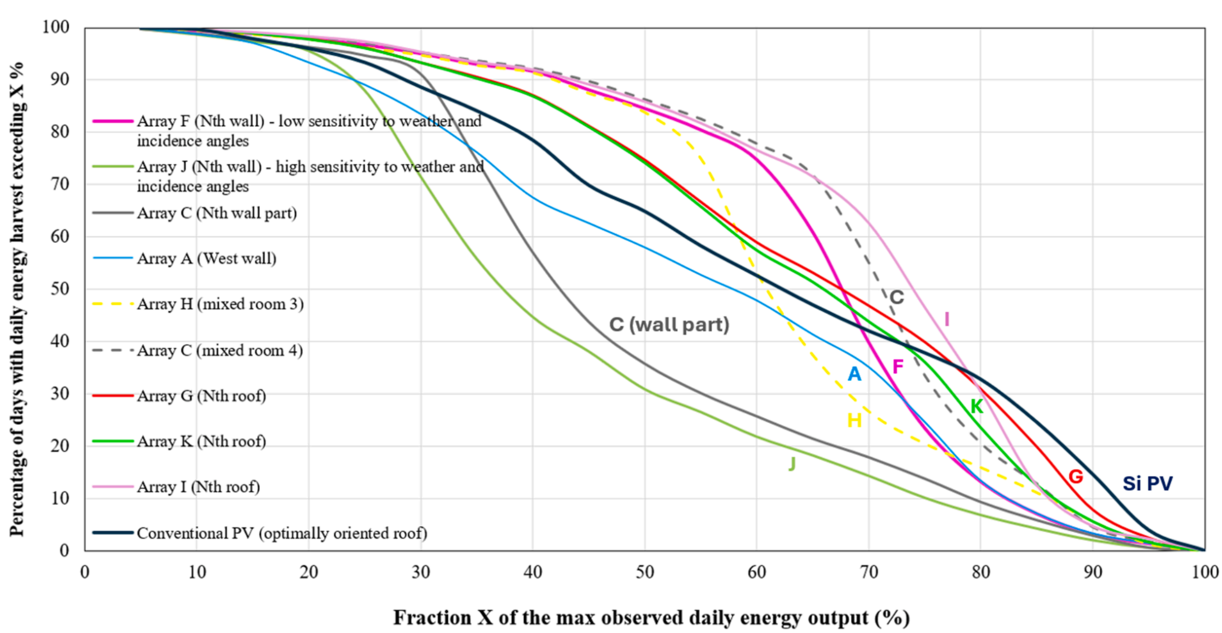

Fig. 3. Overall (season-averaged) array-based statistics trends for the daily energy harvesting data collected between 01 May 2021 – 27 May 2024 from Murdoch University solar greenhouse. The daily energy production data from a conventional 6.6 kW silicon PV system mounted on a 22° tilted NW-oriented roof in Perth were collected (for the same period) from a Fronius SolarWeb online monitoring interface. The data for the wall-mounted fraction of Array C were estimated by subtracting the roof-area-averaged (data from arrays D and E, room 4) estimated contribution of 6 roof-mounted windows from the total measured output of Array C.

The data region near the boundary of the top 40 % of daily energy outputs reveals the performance advantages of all roof-mounted and mixed-array WIPV compared with standard PV, manifesting as the higher probabilities of better energy-output performance in less-than-ideal weather or irradiation conditions.

Fig. 4 shows the measured daily energy production data (normalized to the maximum observed daily energy) collected over 800 days starting from 01 May 2021, for a roof-mounted Array G, in comparison with the same dataset collected from a standard 6.6 kW_p PV system mounted on a 22° tilted NW facing roof (also located within the same metropolitan area). It can be noted that Array G outperformed the conventional PV system quite consistently throughout most of the observation period, and particularly during the autumn, spring, and winter seasons and during most days with adverse weather conditions.

The moving-average data trendlines of Fig. 4(b) highlight the data dependence clearly, also showing that during the summer seasons, the conventional PV array demonstrates better energy harvesting stability and clearly outperforms Array G during the hottest parts of summer. Fig. 5 shows a 1-year dataset for the greenhouse installation-total daily energy harvesting outputs and the yearly total energy production

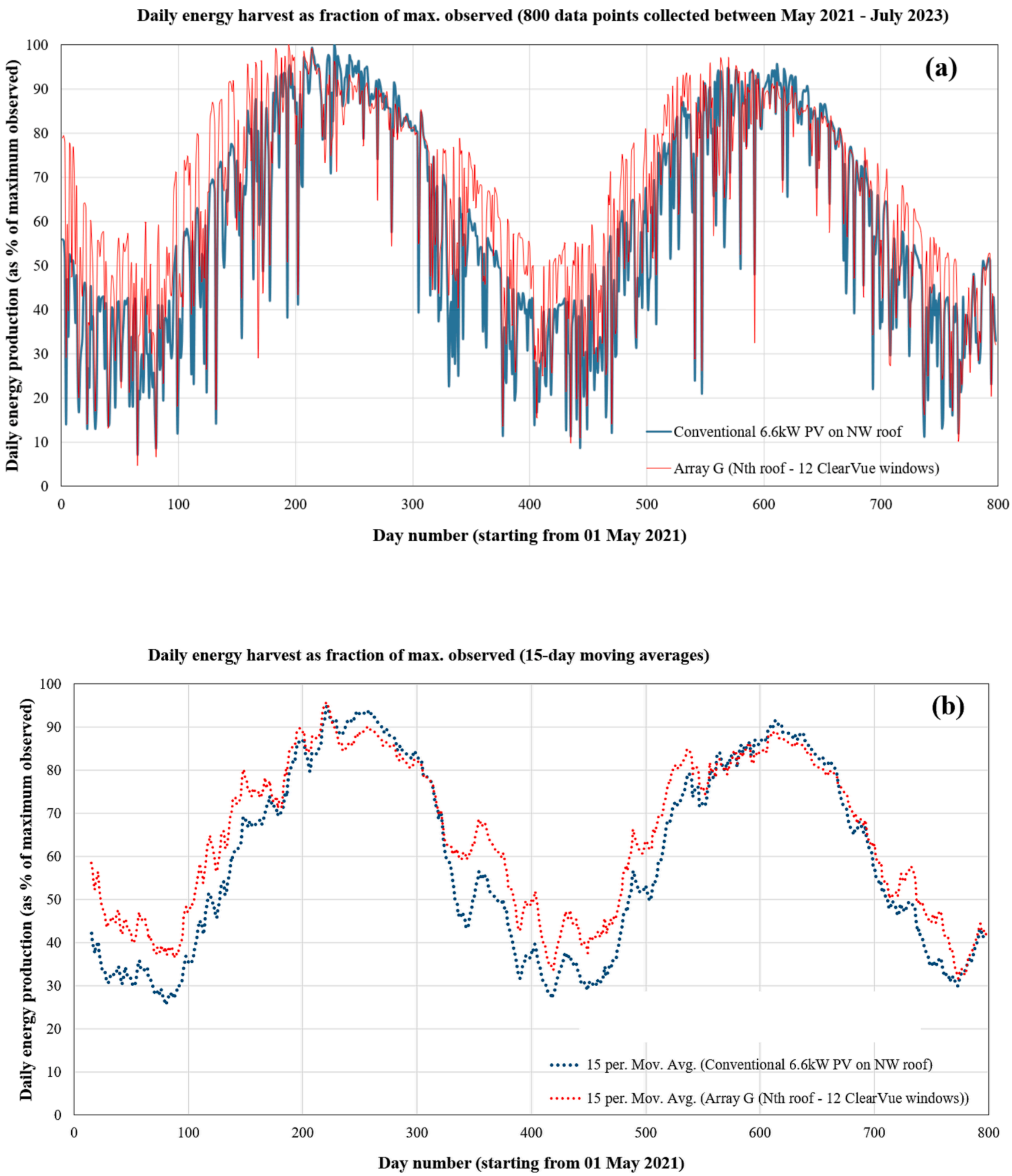

Fig. 4. Systematic energy production performance of a roof-mounted WIPV array compared with a conventional roof-mounted PV system, observed on most adverse-weather days. **(a)** Raw daily energy production data (peak-normalized) collected between May 2021-July 2023; **(b)** The same peak-normalized datasets represented as moving average trendlines with a 15-day period.

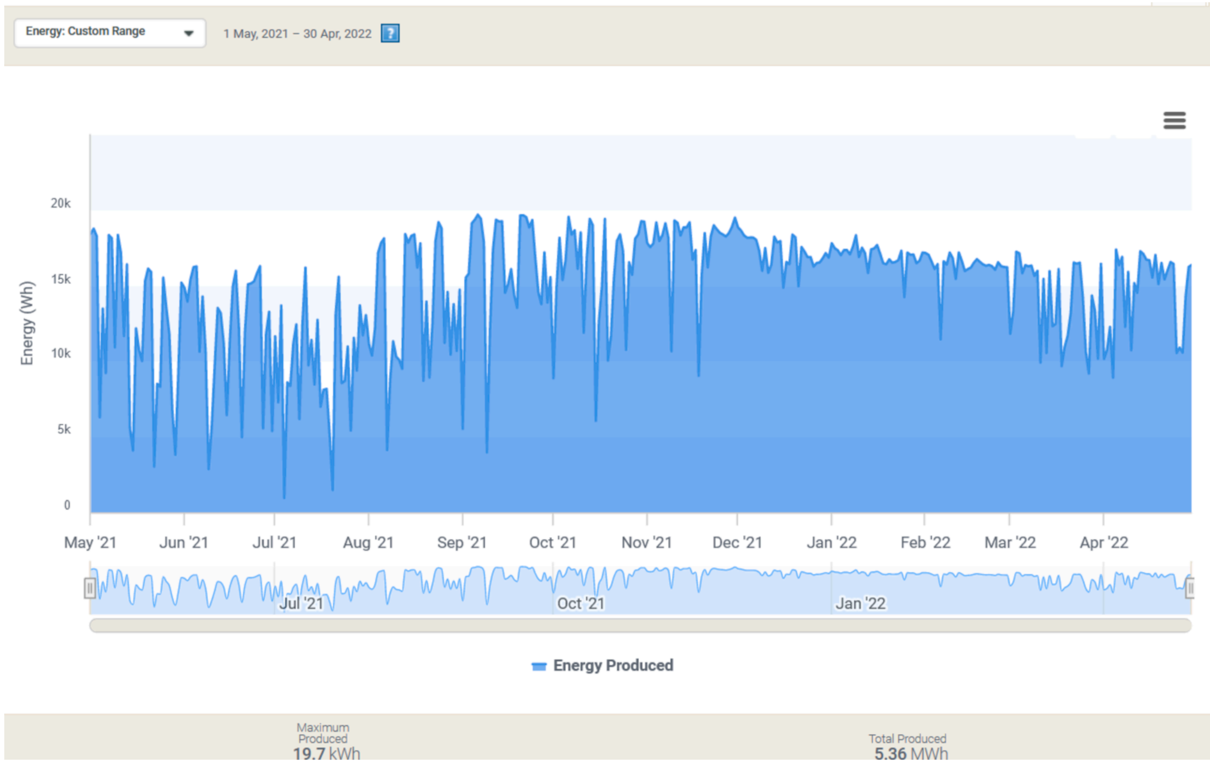

Fig. 5. Relative seasonal stability of the greenhouse-total daily energy output seen on clear-weather days in a multi-oriented window-integrated PV system of greenhouse.

summary. It can be seen from the data of Fig. 5 that the daily energy production remained quite stable throughout seasons, particularly if considering the sunny-day data points measured during winter months; the warmer-seasons' daily production was only minimally affected by the significant noon-time Sun altitude angle variations. Considering that the greenhouse WIPV installation had 63 vertical wall-mounted windows (41.2 % of total), this energy output stability result is also notable. According to the data reported recently in [48], for the conventional PV installations at latitudes between 25° and 45°, the vertical output ranges from 60 to 80 % of the optimum. NREL's PVWatts calculator predicts that (on an average meteorological year for conventional PV installations located in Perth, Australia (greenhouse latitude 32°), a 1kWp system will output 957 kWh/yr if installed onto a vertical north-facing wall. The predicted energy output from the same system installed onto a 22° tilted north-facing roof is 1685 kWh/yr, suggesting that the expected vertical-wall PV outputs are operating at 57 % of the optimum.

Comparing the measured yearly (01 May 2021–01 May 2022) energy outputs of the north wall-mounted 12-window arrays J (310 kWh/yr) and F (399 kWh/yr) with their nearby roof counterparts of identical design type M (494 kWh/yr) and G (507 kWh/yr), the vertical-wall energy performance scaling factors were at 62.75 % (Array J) and 78.7 % (Array F). These differences are window design-related, reflecting the effects of factors such as fluorescence and scattering, particularly important during the summer seasons, when sunlight with the strongest UV and shortwave visible intensities is intercepted by the wall windows at large oblique angles.

3.2. Season-dependent and weather-dependent energy harvesting

It is of interest to analyze the season-specific performance differences and data trends. The combined 3-winter datasets were generated from the dates ranging between 01 June – 31 August during each of the three observation years (2021–2023); summer-specific datasets were generated for the dates between 01 December through to the end of February for all corresponding summer dates starting from December 2021 through to 29 February 2024.

Fig. 6 provides comparisons between the overall (long-term, season-averaged) and winter-seasons' daily energy production data trends, highlighting the significant winter-time reductions in the top-quintile daily energy harvesting probabilities observed in both the conventional PV and the (overall best-performing, eg Array G) roof-mounted WIPV. At the same time, the north-facing wall-mounted and mixed (Array H) window arrays all exhibit significantly higher stability during winter seasons, compared to conventional PV. Roof-mounted windows from Array G consistently outperformed the conventional PV system on adverse-weather days from the data regions below the top 30 % of daily energy outputs, producing higher daily outputs more frequently on cloudy or rainy days.

Windows from the wall-mounted arrays J and F featured more than double the number of days with generation in the top 10 %, compared to the conventional (roof mounted) PV. This was not due only to the vertical mounting orientation being conducive to energy harvesting at lower Sun altitude angles, since the mixed roof-wall Array H has still significantly outperformed the wall windows across the top 25 % energy production range. Interestingly, in the region between the top 50 % and top 75 % of daily winter-time energy outputs, windows from arrays F and H have outperformed even the season-averaged data trend measured with conventional PV. The performance differences between wall-mounted Array J and the conventional PV system depended very strongly on whether the datasets were season-averaged or winter-specific, suggesting significant incidence-angle dependence of the power output from Array J windows. This was also confirmed by the direct performance comparisons between Array J and the wall-mounted windows from other arrays made during summer seasons and could be explained by the design of Array J windows employing a double interlayer structure with greater concentrations of fluorescent particles, likely causing angle-dependent cross-talk between the effects of fluorescence and scattering. The performance differences of LSC

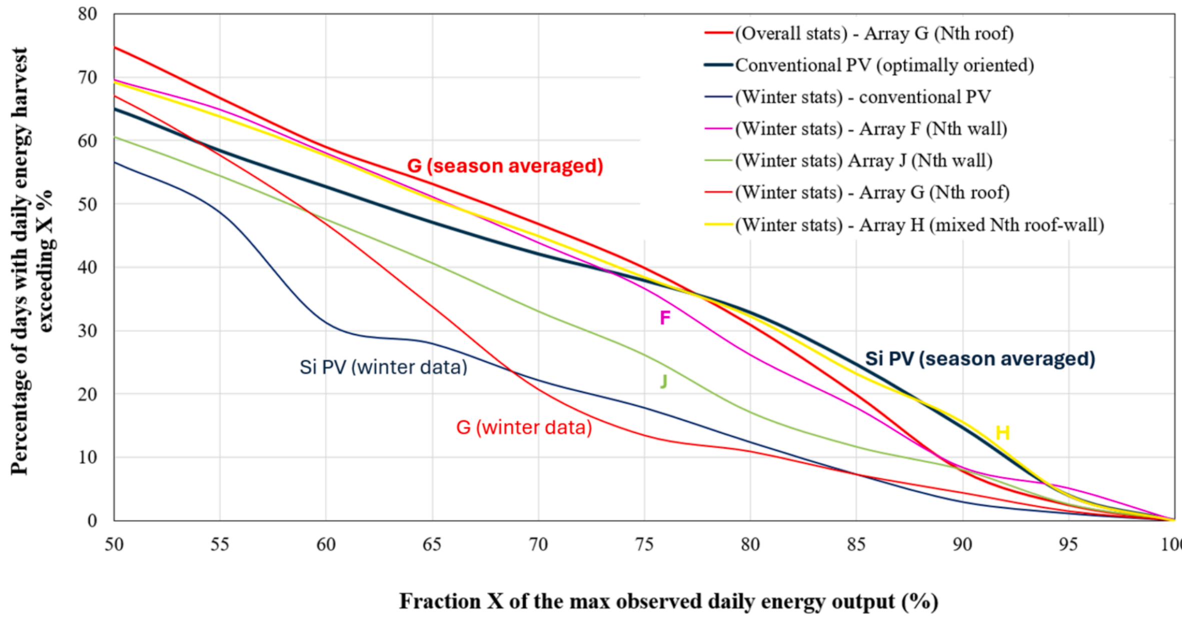

Fig. 6. Comparisons between the overall (long-term, season-averaged) and daily energy production data trends in winter between the conventional roof-mounted PV system and several of the window-integrated PV arrays mounted across the greenhouse building envelope.

components (fluorescent interlayers) relevant to the energy collection efficiency in PV windows are most apparent during the times of peak energy harvesting, when the intensity of excitation-band sunlight (eg. UV-violet) is close to its maximum. Therefore, data comparisons (using Fig. 6) made within the top 5 % subset of the maximum-observed daily energy outputs range can be used to reveal the (mainly) fluorescence-related performance differences between the different wall-mounted window groups. For example, windows from Array F generated daily outputs within their top 5 % approximately two times more often during the winter seasons, compared with Array J.

Fig. 7 shows the energy production data trend comparisons between the summer and winter seasons, revealing a greater inter-season energy harvesting behavior variability of conventional PV, compared to WIPV, across a wide range of environmental conditions. Notably, the wall-mounted Array F and mixed Array H outperformed the conventional roof-mounted PV during summer seasons in all data regions except only the top ~ 17 % of daily production outputs. This is despite the fact that the summer-time conditions feature high Sun altitude angles near noon throughout most of the season, which strongly favours the energy production from roof-mounted PV. Windows from Arrays G, F, and H featured an identical glazing design type and interlayer materials and generated the daily summer-time outputs in the region of top 15 % following very similar data trends, even despite the differences between the roof and wall-based mounting orientations.

Similarly to the winter observations, the data region from the top 5 % of the maximum daily energy production reveals the significant energy collection performance differences between the wall-mounted windows from arrays F and J; the summer-time peak sunlight intensity conditions

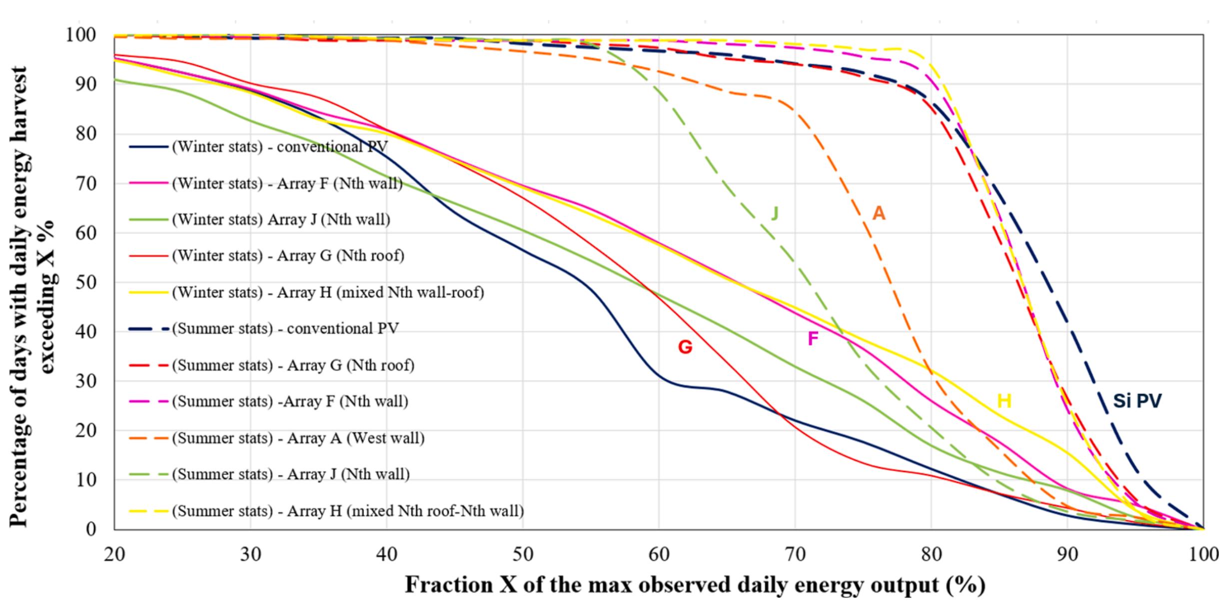

Fig. 7. Comparisons between the season-specific (season-averaged over all of the corresponding 3-month periods between June 2021 and February 2024) daily energy production data trends between the conventional roof-mounted PV and several of the window-integrated PV arrays mounted across the greenhouse building envelope.

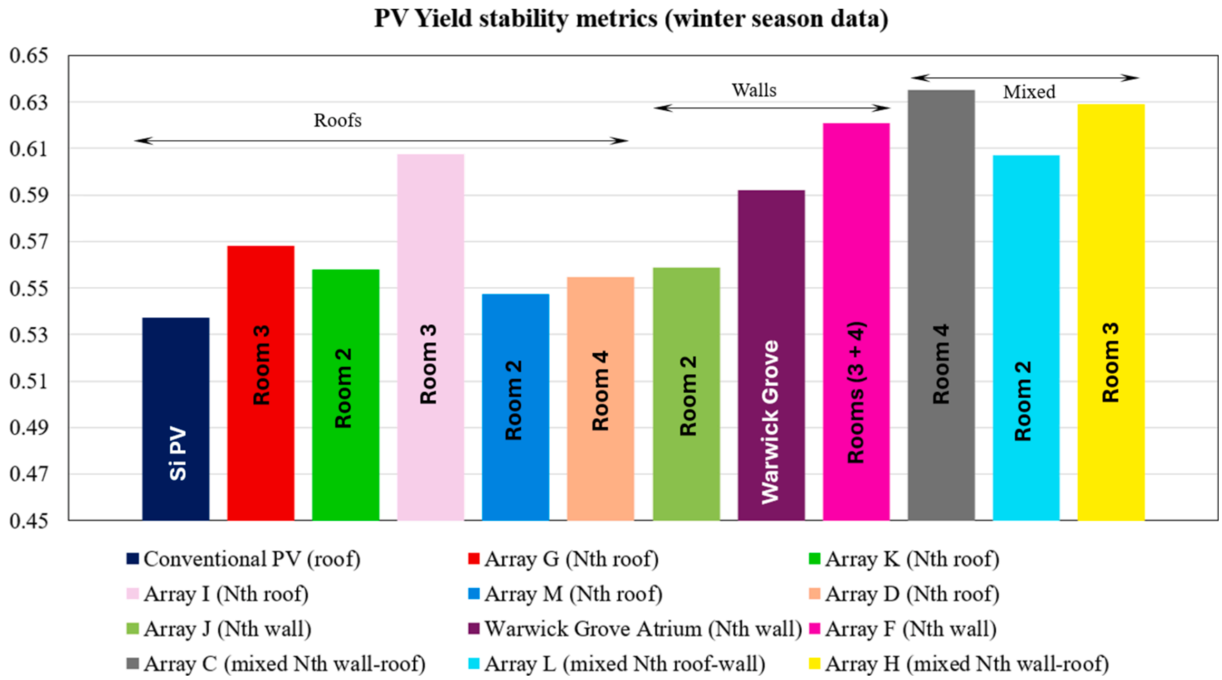

Fig. 8. PV Yield stability metrics comparison between the different window-integrated PV arrays and the conventional roof-mounted NW-oriented silicon PV system. The raw data were collected over the 3 consecutive winter seasons between 2021 and 2023. An additional dataset collected from Warwick Grove shopping centre atrium windows (also located in Perth; the relevant system details were reported in Ref. 16) during its first winter of operation is added for illustration and comparison purposes.

correspond to the large angles of incidence onto vertical walls, which impedes the energy production in systems with lower-quality fluorescent components. Therefore, significant differences are revealed in the observation frequency of top-5 % energy performance in different (but identically oriented) window design types. Similar performance difference results related to the top 5 % and also the top 10–20 % data regions have been identified through long-term energy data analysis for the roof-mounted windows of all three room-specific design types distributed over three separate grow-rooms; these data were reported in [17].

It can be seen from the datasets presented in Figs. 6 and 7 that a conventional, roof-mounted PV system loses its energy harvesting performance in adverse-weather conditions during the winter seasons at a much faster rate, compared to most window-integrated PV types analyzed. We propose to introduce a new energy yield stability (*YS*) metrics parameter to enable the relative rating of the adverse-weather energy harvesting behaviors of different PV, BIPV, and WIPV system types, defined as per Eq.(1). It is best to rate the winter-season system behaviors using this metric, since a larger number of adverse-weather days per unit observation-period duration will then be experienced, contributing to a statistically more accurate real-world system performance evaluation.

$$YS = \frac{E_{seasontotals}}{(E_{peak,1-day} \times N_{days})} \tag{1}$$

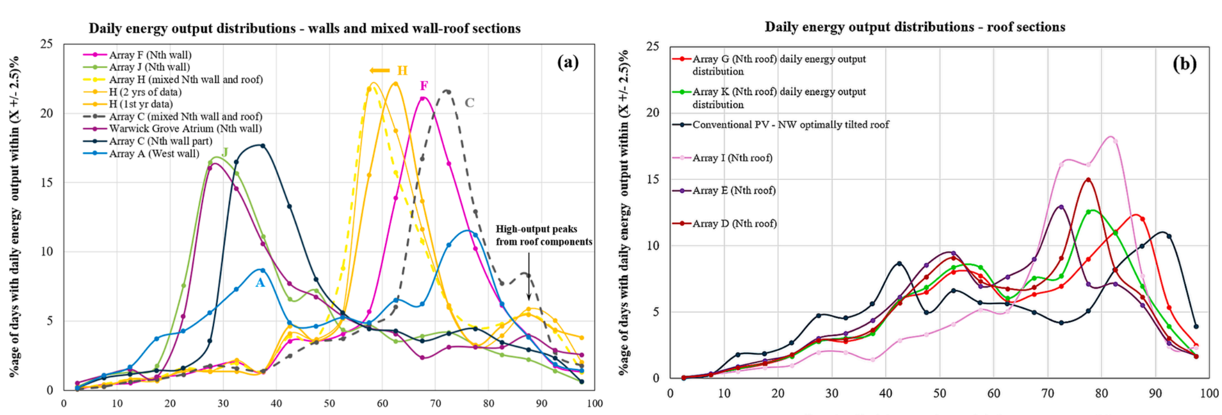

Fig. 9. Per-window daily energy output distributions of the wall-mounted and evenly mixed (roof-wall) (a) and roof-mounted (b) PV window arrays. Greenhouse PV arrays daily energy production data were analyzed during the period between 01 May 2021 – 27 May 2024, to generate the probability distributions of the daily per-window energy outputs being at within ± 2.5 % from a set X% of their maximum-observed daily energy outputs. The data distribution results for array H are shown for three different data collection period limits (data processed within the 1-year and 2-year time-frames, and the total of the observation period), demonstrating both the consistency of the distribution shape, and also some drift in the distribution peak happening over time. Warwick Grove shopping centre atrium (Ref. 16) data from its 8 windows mounted on its north facing wall were collected during the 1st year of atrium operation; these data are included in part (a) for comparison purposes.

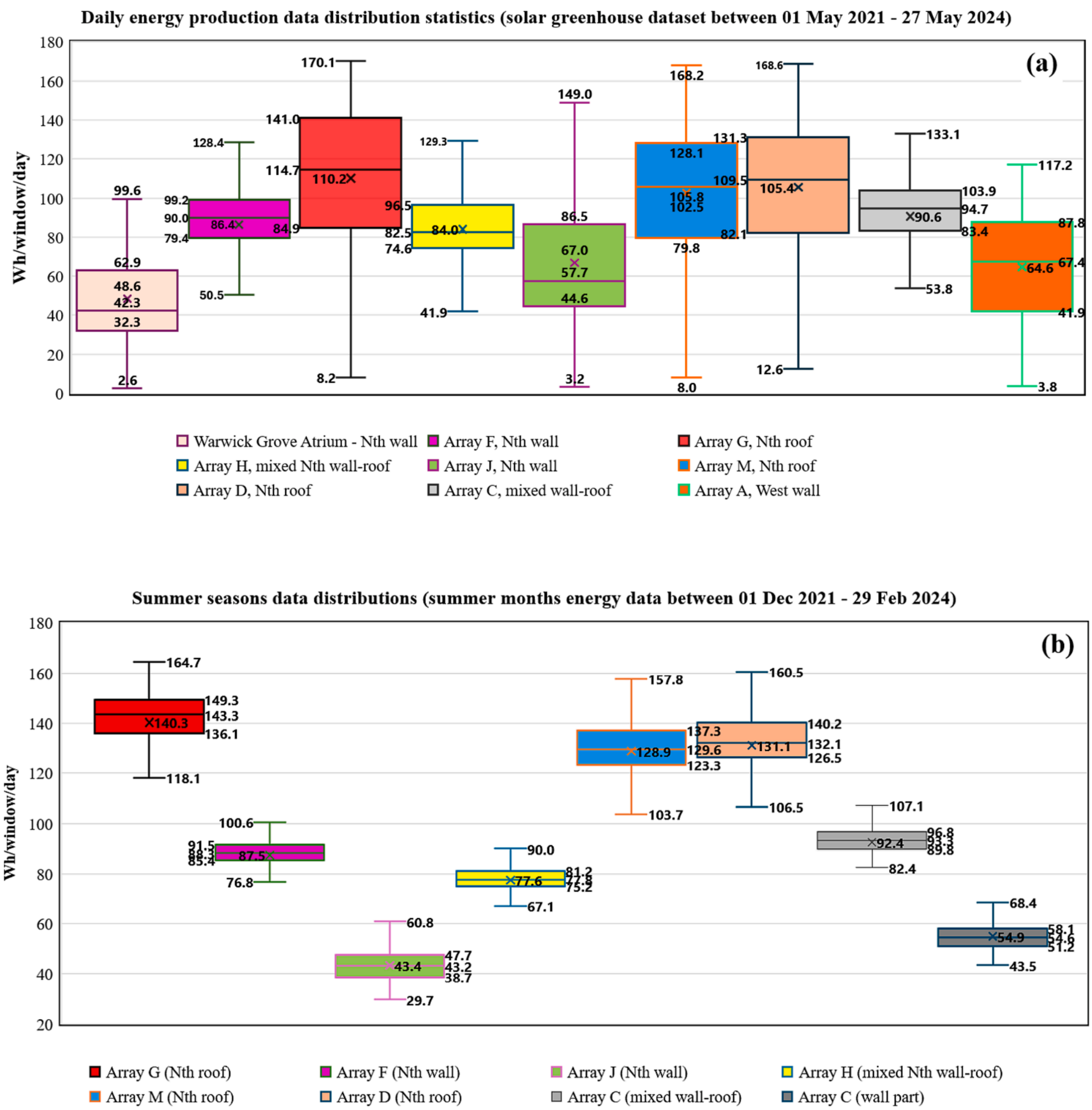

Fig. 10. Plots of the per-window daily energy production data distribution statistics measured from different greenhouse window arrays over the period between 01 May 2021 – 27 May 2024 (with Warwick Grove data limited to its first year of operation) **(a)**; the summer-season energy harvesting data distributions plotted separately for the 276 summer data points collected between 01 Dec 2021 – 29 Feb 2024 **(b)**.

where $E_{season\ totals}$ is the total amount of energy produced by the PV module (or a PV window array) during the observation period, $E_{peak,\ 1-day}$ is the maximum daily energy produced during the observation period, and N_{days} is the total number of days. This energy yield stability parameter YS essentially quantifies the season-total generated energy as a fraction of its "theoretical maximum", which would have been recorded if every day during the entire observation period was identical in solar radiation exposure conditions and weather parameters to the "day of maximum energy production" recorded during the period.

Fig. 8 shows the results of the PV Yield stability metrics evaluation made for several window arrays mounted across the Murdoch greenhouse building envelope using the energy data collected from 276 winter days in 2021–2023; the stability metrics data for a group of 8 north-wall windows of another WIPV installation in Perth (Warwick Grove shopping centre atrium) were processed only for its first winter of operation in 2019.

It is notable that all north-oriented window-integrated PV arrays outperformed the conventional, roof-mounted silicon panels in terms of the stability parameter proposed in Eq. (1). The results also show that WIPVs exhibit improved stability for systems mounted on vertical walls and the mixed-orientation (wall-roof) window arrays. Another way of analyzing the long-term monitored daily energy outputs from different PV systems involves generating the probability distributions of different daily energy production amounts.

Energy output intervals can be sampled in small (5 % of the maximum observed) steps, eg by plotting the percentage of the total number of days corresponding to the daily energy outputs belonging to the intervals of within ± 2.5 % from a set value, expressed in terms of the maximum-observed daily energy output. Fig. 9 shows the probability distributions of daily energy outputs (normalized to the maximum observed), obtained through the analysis of long-term continuous energy data observations, presented separately for the different wall-mounted and roof-mounted WIPV and PV systems.

It is noted from the graphs of Fig. 9 that the energy output distributions feature characteristic peaks, which can be used to rate the energy harvesting performance of different PV arrays. The three distributions plotted for Array H using the 1-year, 2-year, and 3-year daily energy production datasets show that the overall distribution shape remains the same. However, there is a notable drift in the peak position towards lower energies over time, attributed to gradual dust accrual occurring after the first year of operation. Mixed wall-roof window arrays also feature small higher-energy output distribution peaks likely generated by the contributions of their roof-mounted sections.

The plots in Fig. 10 show the season-averaged (a) and summer season-specific (b) daily energy production distribution parameters measured from each of the PV window arrays shown.

The parameters (distribution averages, mean values, and the data quintile boundaries) shown in the plots of Fig. 10 resolve the statistically significant design-dependent differences between the different distributions plotted for either the roof-, wall-mounted, or mixed-orientation window arrays. All window types analyzed were of area 1.32 m^2 but differed slightly in their fluorescent interlayer design parameters (primarily the particle size distributions and their concentrations). The wall-mounted arrays exhibited stronger energy harvesting differences. Energy production data distributions specific to summer seasons showed greater energy harvesting performance differences between the roof-mounted and wall-mounted windows. This was expected, due to much larger frequency of days conducive to effective energy harvesting during the summer seasons. Array H data showed some unexpected weaker performance compared with Array F, possibly indicating the presence of some technical window-related issues, or extensive contamination. The proposed methodologies for the field performance analysis of building-integrated PV are expected to expand the arsenal of techniques suitable for benchmarking unconventional PV modules and installations.

Finally, we note that these LSC characterization experiments have revealed substantial interlayer composition-dependent and thickness-dependent differences in light collection performance. Adding an aluminium backreflector layer to the LSC structure led to much larger energy collection in fluorescent samples, compared with a "blank" reference window. This was expected, due to the back-reflection effects stimulating multi-pass propagation through luminescent interlayers.

The best performance was achieved in this study using a low-haze (several %), high-transparency 100 mm x 100 mm x 9 mm window featuring approximately 85 % of color-unbiased visible light transmission with a 0.76 mm "PVB-A" interlayer. For these windows, we found a PCE = 1.12 % and optical power efficiency (the ratio of edge-escaping optical power to the power incident onto entire LSC glass area) in excess of 7 %. These data were obtained from measurements using 4 edge-attached silicon cells of only 16 % nominal efficiency and capturing the light escaping through edge areas only. The measured LSC sample performance metrics are among the highest reported so far for LSCs of similar dimensions, haze, and visible-range optical transparency.

4. Conclusions

Ongoing developments in the fields of BIPV and unconventional photovoltaics, including high-transparency window-integrated PV, continue to be reported worldwide. Novel energy-efficient, energy-generating window-integrated PV products and technologies are starting to demonstrate their applicability on an industrial scale, and the feasibility of their commercialization, in both the commercial buildings and agrivoltaics sectors. The results reported have shown that "transparent", i.e. colourless LSC-based windows can generate significant electricity, and this has been corroborated in this paper through the first large pilot scale demonstration plant, which has successfully run with no significant power losses for over three years. Experimental findings demonstrate that solar energy harvesting windows exhibit advantages over conventional silicon module-based PV systems, particularly if installed onto vertical wall surfaces or subjected to adverse weather conditions. The development of statistical methods suitable for evaluating the energy collection behaviour of LSC based windows has been reported. The methods described rely on the availability of the long-term daily energy production data records, and require the analysis of data generated during multiple seasons and weather conditions, in order to reveal the details of system-dependent energy harvesting behaviour trends. These methodologies can enable the identification of the best-performing window-integrated PV designs, as well as benchmarking the energy conversion characteristics of different PV, BIPV, and other renewable energy technologies.

Author contributions

Conceptualization, M.V. and V.R.; methodology, M.V., P.M. and J.B.; validation, P.M. and V.R.; investigation, M.V., J.B. and P.M.; writing—original draft preparation, M.V.; writing—review and editing, P.M. and J.B.; materials development and manuscript editing, P.M.; supervision, P.M. and V.R.; project administration, V.R. All authors have read and agreed to the published version of the manuscript.

CRediT authorship contribution statement

Mikhail Vasiliev: Writing – review & editing, Writing – original draft, Methodology, Investigation, Conceptualization. **Victor Rosenberg:** Validation, Supervision, Conceptualization. **James Bullock:** Writing – review & editing, Methodology, Investigation. **Paul Mulvaney:** Writing – review & editing, Validation, Supervision, Methodology, Investigation.

Funding

This research received no external funding.

Declaration of Competing Interest

The authors declare that they have no known competing financial interests or personal relationships that could have appeared to influence the work reported in this paper.

Acknowledgments

The authors would like to acknowledge the contributions of Dr Di Yan and Qingrui Kong, who worked as part of the Exciton Science research team at the University of Melbourne, for assistance with the materials characterization and PV measurement experiments conducted during this study. PM thanks the ARC for support through grant CE170100026.

References

[1] World Energy Outlook 2023; IEA Publications, International Energy Agency: Paris, France, **2023**; Available online: https://www.iea.org/reports/world-energy-outlook-2023 (sighted on 11 June 2024).
[2] Kiss Cathcart Anders Architects. NREL Study: Building-Integrated Photovoltaics. **1993** NREL publication, PC 1993, 1-59. Available online: https://www.google.com/url?sa=t&source=web&rct=j&opi=89978449&url=https://kisscathcart.com/pdf/BIPV1kc.pdf&ved=2ahUKEwiziYGA6dKGAxVNT2wGHahUDUUQFnoECCkQAQ&usg=AOvVaw25nkwg3sz89c3qKO5TPjpj (sighted on 11 June 2024).
[3] R.A.M. Lameirinhas, J.P.N. Torres, J.P. de Melo Cunha, A Photovoltaic Technology Review: History, Fundamentals and Applications, Energies (1823, 2022,) 15.
[4] D.S. Pillai, V. Shabunko, A. Krishna, A comprehensive review on building integrated photovoltaic systems: Emphasis to technological advancements, outdoor testing, and predictive maintenance, Renew. Sust. En. Rev. 156 (2022) 111946.
[5] J. Peng, H. Goudey, A. Thanachareonkit, C. Curcija, E. Lee, MEASUREMENT & VERIFICATION OF THE PERFORMANCE OF SOLARIA BIPV IN FLEXLAB TEST FACILITY, Lawrence Berkeley National Laboratory Publication (2017) 1–77.
[6] M. Vasiliev, M. Nur-E-Alam, K. Alameh, Recent Developments in Solar Energy-Harvesting Technologies for Building Integration and Distributed Energy Generation, Energies 12 (2019) 1080.

[7] A. Borja Block, J.E. Palou, M. Courtant, A. Virtuani, G. Cattaneo, et al., Colouring solutions for building integrated photovoltaic modules: A review, Energ. Buildings 314 (2024) 114253.
[8] A. Anctil, M.N. Beattie, C. Case, A. Chaudhary, B.D. Chrysler, M.G. Debije, et al., Status report on emerging photovoltaics, J. Photon. En. 13 (4) (2023).
[9] K. Lee, H.-D. Um, D. Choi, J. Park, N. Kim, H. Kim, K. Seo, The Development of Transparent Photovoltaics, Cell Rep. Phys. Sci. 1 (2020) 100143.
[10] M. Vasiliev, V. Rosenberg, D. Goodfield, J. Lyford, C. Li, High-transparency clear window-based agrivoltaics. Sust, Build. 6 (2023) 5.
[11] J. Huang, J. Zhou, E. Jungstedt, A. Samanta, J. Linnros, L.A. Berglund, I. Sychugov, Large-Area Transparent "Quantum Dot Glass" for Building-Integrated Photovoltaics, ACS Photonics 9 (2022) 2499–2509.
[12] F. Meinardi, F. Bruni, C. Castellan, M. Meucci, A.M. Umair, M. La Rosa, J. Catani, S. Brovelli, Certification Grade Quantum Dot Luminescent Solar Concentrator Glazing with Optical Wireless Communication Capability for Connected Sustainable Architecture, Adv. Energy Mater. 14 (2024) 2304006.
[13] T.A. De Bruin, R. Terricabres-Polo, A. Kaul, N.K. Zawacka, P. Tim Prins, T.F. J. Gietema, A.C. de Waal, D.K.G. de Boer, D.A.M. Vanmaekelbergh, L.P. Leblans, et al., Analysis of the 1 Year Outdoor Performance of Quantum Dot Luminescent Solar Concentrators, Sol. RRL 7 (2023) 2201121.
[14] ClearVue Technologies Website. Available online: https://www.clearvuepv.com/resources/ (accessed on 01 September 2024).
[15] Alameh, K.; Rosenberg, V.; Vasiliev, M. Device for generating electric energy. Patent US11162302B2, 2 November 2021. Available online: https://patents.google.com/patent/US11162302B2/en (accessed on 20 June 2024).
[16] M. Vasiliev, M. Nur-E-Alam, K. Alameh, Initial Field Testing Results from Building-Integrated Solar Energy Harvesting Windows Installation in Perth, Australia. Appl. Sci. 9 (2019) 4002.
[17] M. Vasiliev, V. Rosenberg, J. Lyford, D. Goodfield, Field Performance Monitoring of Energy-Generating High-Transparency Agrivoltaic Glass Windows, Technologies 11 (4) (2023) 95.
[18] V.M. Wheeler, J. Kim, T. Daligault, B.A. Rosales, C. Engtrakul, R.C. Tenent, L. M. Wheeler, Photovoltaic windows cut energy use and CO_2 emissions by 40% in highly glazed buildings, One Earth 5 (11) (2022) 1271–1285.
[19] J.-H. Kim, S.-K. Son, G.-S. Choi, Y.-T. Kim, S.-B. Kim, W.-K. Choi, A Fundamental Study on the Development of New Energy Performance Index in Office Buildings, Energies 14 (2021) 2064.
[20] G.E. Samanoudy, N.S.A. Mahmoud, C. Jung, Analyzing the effectiveness of building integrated Photovoltaics (BIPV) to reduce the energy consumption in Dubai, Ain Shams Eng. J. 15 (2024) 102682.
[21] M.G.S. Conde, K. Shanks, Evaluation of Available Building Integrated Photovoltaic (BIPV) Systems and their Impact when Used in Commercial Buildings in the United Arab Emirates, Int. J. Sust. En. Dev. 7 (1) (2019) 344–356.
[22] M. Abdelhakim, J.D. Jibril, M.Z. Kandar, Y.A. Dodo, Low Carbon Emission through the Use of BIPV Windows in Algerian Mid-Rise Buildings, Chem. Eng. Transact. 56 (2017) 541–546.
[23] P.K. Tawalare, Optimizing Photovoltaic Conversion of Solar Energy, AIP Adv. 11 (2021) 100701.
[24] S. Castelletto, A. Boretti, Luminescence solar concentrators: A technology update, Nano Energy 109 (2023) 108269.
[25] R. Alghamedi, M. Vasiliev, M. Nur-E-Alam, K. Alameh, Spectrally-Selective All-Inorganic Scattering Luminophores For Solar Energy-Harvesting Clear Glass Windows, Sci. Rep. 4 (2014) 6632.
[26] Y. Zhang, Z. Zheng, X. Cao, J. Song, Z. Gan, R. Huang, X. Zhang, Quantifying Mie Scattering in Luminescent Solar Concentrators for Improved Performance, ACS Photonics 10 (9) (2023) 3095–3104.
[27] C. Corrado, S.W. Leow, M. Osborn, E. Chan, B. Balaban, S.A. Carter, Optimization of gain and energy conversion efficiency using front-facing photovoltaic cell luminescent solar concentrator design, Sol. Energy Mater. Sol. Cells 111 (2013) 74–81.
[28] T.K. Baikie, B. Daiber, E. Kensington, J. Xiao, N.C. Greenham, B. Ehrler, A. Rao, Revealing the potential of luminescent solar concentrators in real-world environments, Joule 8 (2024) 1–18.
[29] T. Warner, K.P. Ghiggino, G. Rosengarten, A critical analysis of luminescent solar concentrator terminology and efficiency results, Sol. Energy 246 (2022) 119–140.
[30] S. Han, J. Wen, Z. Cheng, G. Chen, S. Jin, et al., Luminescence-guided and visibly transparent solar concentrators based on silicon quantum dots, Opt. Express 30 (15) (2022) 26896–26911.
[31] F. Zhang, J. Bao, C. Gao, Design and Optimization of Transparent Scattering Solar Concentrator based on SiO_2 Aerogel, JUSTC 52 (10) (2022) 2, https://doi.org/10.52396/JUSTC-2022-0047.
[32] M. Polché, B.F.J. Miguel, C.A.G. González, G.G. Contreras, V.H.R. Arellano, Study of the Scattering Effect by SiO_2 Nanoparticles, in a Luminescent Solar Concentrator Sensitized with Carbon Dots, Nanomaterials 13 (2023) 2480.
[33] A.M. Ramachandran, M.S. Sangeetha, A.S. Thampi, M. Singh, A. Asok, A comprehensive review on optics and optical materials for planar waveguide-based compact concentrated solar photovoltaics, Results Eng. 16 (2022) 100665.
[34] Y.C. Demir, M.A. Aktacir, Experimental Investigation of the BIPV System under Şanlıurfa Meteorological Conditions, Appl. Sci. 13 (2023) 11286.
[35] N.M. Kumar, M. Samykano, A. Karthick, Energy loss analysis of a large scale BIPV system for university buildings in tropical weather conditions: A partial and cumulative performance ratio approach, Case Stud. Therm. Eng. 25 (2021) 100916.
[36] E. Ela, V. Diakov, E. Ibanez, M. Heaney, Impacts of Variability and Uncertainty in Solar Photovoltaic Generation at Multiple Timescales; Technical Report NREL/TP-5500-58274; NREL: Golden, CO, USA, 2013.
[37] M.A. Imteaz, A. Ahsan, Solar panels: Real efficiencies, potential productions and payback periods for major Australian cities, Sust. Energy Technol. Assessm. 25 (2018) 119–125.
[38] M. Siripurapu, F. Meinardi, S. Brovelli, F. Carulli, Environmental Effects on the Performance of Quantum Dot Luminescent Solar Concentrators, ACS Photonics 10 (2023) 2987–2993.
[39] M.G. Debije, V.A. Rajkumar, Direct versus indirect illumination of a prototype luminescent solar concentrator, Sol. Energy 122 (2015) 334–340.
[40] M. Vasiliev, R. Alghamedi, M. Nur-E-Alam, K. Alameh, Photonic microstructures for energy-generating clear glass and net-zero energy buildings, Sci. Rep. 6 (2016) 31831.
[41] R.A.S. Ferreira, S.F.H. Correia, P. Georgieva, L. Fu, M. Antunes, P.S. André, A comprehensive dataset of photonic features on spectral converters for energy harvesting, Sci. Data 11 (2024) 50.
[42] H. Zhao, G. Liu, G. Han, High-performance laminated luminescent solar concentrators based on colloidal carbon quantum dots, Nanoscale Adv. 1 (2019) 4888.
[43] C. Yang, et al., Consensus statement: Standardized reporting of power-producing luminescent solar concentrator performance, Joule 6 (1) (2022) 8–15.
[44] G. Liu, R. Mazzaro, C. Sun, Y. Zhang, Y. Wang, H. Zhao, G. Han, A. Vomiero, Role of refractive index in highly efficient laminated luminescent solar concentrators, Nano Energy 70 (2020) 104470.
[45] S. Verma, D.J. Farrell, R.C. Evans, Ray-Trace Modeling to Characterize Efficiency of Unconventional Luminescent Solar Concentrator Geometries, ACS Appl. Opt. Mater. 1 (2023) 1012–1025.
[46] M. Cao, X. Zhao, X. Gong, Achieving High-Efficiency Large-Area Luminescent Solar Concentrators, JACS Au 3 (1) (2023) 25–35.
[47] R.A.S. Ferreira, S.F.H. Correia, A. Monguzzi, X. Liu, F. Meinardi, Spectral converters for photovoltaics—What's ahead, Mater. Today 33 (2020) 105–121.
[48] W.O. Al-Rashidy, A.A. Azooz, Efficiency of Vertically Installed Solar PV Panels, Appl. Sol. Energy (2024), https://doi.org/10.3103/S0003701X24600164.